Polymorphism in the assembly of polyomavirus capsid protein VP_1

D. M. Salunke,* D. L. D. Caspar,* and R. L. Garcea‡
*Rosenstiel Basic Medical Sciences Research Center, Brandeis University, Waltham, Massachusetts 02254-9110; and
‡Division of Pediatric Oncology, Dana Farber Cancer Institute and Children's Hospital, Boston, Massachusetts 02115

ABSTRACT Polyomavirus major capsid protein VP_1, purified after expression of the recombinant gene in *Escherichia coli,* forms stable pentamers in low-ionic strength, neutral, or alkaline solutions. Electron microscopy showed that the pentamers, which correspond to viral capsomeres, can be self-assembled into a variety of polymorphic aggregates by lowering the pH, adding calcium, or raising the ionic strength. Some of the aggregates resembled the 500-Å-diameter virus capsid, whereas other considerably larger or smaller capsids were also produced. The particular structures formed on transition to an environment favoring assembly depended on the pathway of the solvent changes as well as on the final conditions. Mass measurements from cryoelectron micrographs and image analysis of negatively stained specimens established that a distinctive 320-Å-diameter particle consists of 24 close-packed pentamers arranged with octahedral symmetry. Comparison of this unexpected octahedral assembly with a 12-capsomere icosahedral aggregate and the 72-capsomere icosahedral virus capsid by computer graphics methods indicates that similar connections are made among trimers of pentamers in these shells of different size. The polymorphism in the assembly of VP_1 pentamers can be related to the switching in bonding specificity required to build the virus capsid.

INTRODUCTION

The polyomavirus capsid is built of 72 capsomeres that are all pentamers of the major capsid protein VP_1 (Rayment et al., 1982). The 12 pentavalent and 60 hexavalent capsomeres are arranged in the positions of the 5- and 6-coordinated vertices of a $T = 7d$ icosahedral surface lattice (Caspar and Klug, 1962). If the 60 hexavalent capsomeres had been hexamers, as initially proposed on the basis of the morphology (Klug, 1965), then all the protein molecules could have been quasiequivalently related, in accord with the theory that bonding specificity should be conserved in icosahedral surface lattices (Caspar and Klug, 1962). However, because all 72 capsomeres are pentamers, VP_1 molecules must be nonequivalently bonded in the icosahedral capsid structure. The basic question about the assembly of the polyomavirus capsid posed by its structure is: how do the VP_1 molecules in the pentameric capsomeres switch their bonding specificity to fit into the symmetrically distinct environments in the capsid surface lattice?

The ability to purify substantial amounts of the polyomavirus VP_1 protein from *Escherichia coli* after expression of the recombinant gene (Leavitt et al., 1985) has enabled investigation of the intrinsic interaction properties of this molecule. We have shown by electron microscopy that VP_1 is isolated from *E. coli* as pentamers with the same morphology as viral capsomeres, and these pentamers can be self-assembled into capsidlike aggregates (Salunke et al., 1986). The switching to form nonequivalent bonds connecting the pentamers in the self-assembled shells, therefore, must be an inherent property of the VP_1 molecule. The size heterogeneity of these shells formed from purified recombinant VP_1 suggested that the accurate construction of the native 72-pentamer virus capsid may involve accessory control mechanisms. In addition to capsidlike structures, we observed variant aggregates of the self-assembled VP_1 pentamers which resembled polymorphic capsomere assemblies seen in extracts of cells infected with papillomaviruses (Finch and Klug, 1965), polyomavirus (Mattern et al., 1967), and SV40 (Koch et al., 1967). Information about the nature of the forces and the specificity of the bonding that determine the assembly process can be obtained by comparison of the morphology and stability of the polymorphic aggregates which form under different conditions.

Studies on the self-association of tobacco mosaic virus protein (Caspar, 1963; Bloomer and Butler, 1986; Okada, 1986) and icosahedral plant virus proteins (Bancroft, 1970; Argos and Johnson, 1984) as a function of solvent conditions provide precedents for relating the stabilizing interactions and the packing arrangements in different states of assembly. Electrostatic interactions are important in all these assembly processes as evidenced by the sensitivity to ionic conditions. Based on our previous

observations on the self-assembly of the recombinant polyomavirus VP_1 protein (Salunke et al., 1986) and other investigations on the dissociation of purified polyomavirus (Brady et al., 1977; Friedman and David, 1972) and SV40 (Christiansen et al., 1977), we decided to explore the effects of pH, calcium addition, and ionic strength on the packing arrangements and stability of polymorphic aggregates of the VP_1 pentamers. We have concentrated on the interpretation of electron micrographs of specimens prepared under different solvent conditions. We found that the state of assembly of the VP_1 pentamers depended on the pathway of the solvent changes as well as on the final conditions. Image analysis of a distinctive polymorphic shell aggregate has posed unanticipated questions about switching in the symmetry of the pentamer packing arrangements.

METHODS

Protein preparation

VP_1 was purified after expression of the recombinant VP_1 gene of the RA strain in *E. coli* as described previously (Leavitt et al., 1985). The purification was carried out in 10 mM Tris-HCl (pH 7.2) containing 1 mM ethylene diamine tetraacetic acid (EDTA) and 15 mM 2-mercaptoethanol (2-ME) to prevent possible aggregation. The buffers used for the assembly reactions were 10 mM Tris-HCl (pH 8.5 and 7.2) and 10 mM sodium acetate (pH 5.0). All the solutions contained 5% glycerol.

A microdialysis cell was used for dialysis of solutions on the order of 50–100 μl, with no significant loss of the sample. Nine different environmental conditions resulting from variation in pH, ionic strength, and calcium concentration were examined. Protein was equilibrated to a new set of conditions by step-dialysis over 2–3 d. The experiments were carried out at 22°C at protein concentrations between 0.5 and 1.0 mg/ml.

Electron microscopy

The electron micrographs (Figs. 1 and 2) were recorded using EM301 and EM420 electron microscopes (Philips Electronic Instruments, Inc., Mahwah, NJ) operating at 80 and 100 kV, respectively. The conventional procedure adopted for the preparation of grids of negatively stained specimens for electron microscopy has been described previously (Salunke et al., 1986). The sample for cryoelectron microscopy was embedded in a thin layer of vitreous ice using a quick-freezing procedure (Dubochet et al., 1988). The frozen specimens were transferred under liquid nitrogen to a cryospecimen holder (Gatan, Inc., Warrendale, PA). The specimens were examined in a Philips EM420 electron microscope at a temperature of −170°C. The images were recorded with low irradiation (~30e/Å) and 1.0 μm underfocus.

Image processing

Image analysis was carried out on the electron micrographs of the frozen-hydrated specimen for mass measurements and on the negatively stained specimen for image enhancement. The Spider software package (Frank et al., 1981) was used for image averaging.

Several images of the low-irradiation, frozen-hydrated specimen were scanned on a microdensitometer (Optronics International Inc., Chelmsford, MA) with a scanning raster equivalent to 3 Å. For mass measurements, a 320-Å-diameter particle image was circularly averaged as a reference, and the cross-correlation functions were computed between each of the images in the scanned region and the circularly averaged reference. Ten images that correlated well with the reference were selected and the integrated scattering density was calculated after subtracting the average background density for each image. The integrated scattering density for three 500-Å-diameter particles from the same micrograph was similarly calculated. The relative mass of the 320-Å-diameter particle was then calculated from the ratio of the average integrated scattering density of ten 320-Å-diameter images to that of the three 500-Å-diameter images.

The characteristic threefold and fourfold symmetry views of the presumed octahedral particles were visually identified in the micrographs of a negatively stained specimen. Images of the twofold view were identified from comparison with the model based on the views along threefold and fourfold axes (Fig. 3). Nine selected images (four each of three- and fourfold views and one twofold view) were scanned on the microdensitometer and the contrast was enhanced. The centers of the images were identified visually and later refined by the calculation of the rotational power spectrum (Crowther and Amos, 1971). The images were cyclically averaged by applying the corresponding rotational symmetry. Image processing of the presumed $T = 1$ icosahedral particles (Fig. 4) was also carried out by similar procedures.

Model building

Pictures representing the surface morphology of the polyomavirus capsid and polymorphic assemblies of the capsomeres were constructed utilizing the computer graphics system developed for illustrating complex macromolecular assemblies (Namba et al., 1988). The polyomavirus capsid model (Salunke et al., 1986, Figs. 5 and 6) was based on the 22.5 Å resolution electron density map (Rayment et al., 1982). The VP_1 molecules were represented as 80-Å-long rods with rounded ends which were joined together to form a slightly tapered pentamer of mean diameter ~80 Å, corresponding to the observed size and shape of the capsomere. In the model depicting the 500-Å-diameter icosahedral virus capsid, the 72 pentamers were packed together, as in the electron density map, with each protruding domain extending out ~55–60 Å from the surface of close contact.

Models of the 24-capsomere octahedral (24-OCTA) and 12-capsomere icosahedral (12-ICOSA) assemblies (Figs. 3–6) were built using the model pentamer that was constructed to fit the virus capsid structure. With this constraint, the adjustable parameters in the octahedral model were the spherical coordinates of a pentamer axis in the cubic frame, and the position of the model pentamer defined by its radial translation and angular rotation relative to this axis. For the 12-ICOSA model, the adjustable parameters were only the translation and rotation of the pentamer relative to the fixed icosahedral fivefold axis. The model parameters were then adjusted to obtain the best fit with the electron micrographs.

Low-resolution versions of the models of the polymorphic octahedral and icosahedral assemblies were used to simulate images of particles with one surface embedded in a thin layer of negative stain (Figs. 3 and 4, third row). In these models, the capsomere was represented as a hollow Gaussian cylinder. Thus, only its radial position along its axis had to be adjusted. Projection of one hemisphere of a model shell normal to the bisecting plane corresponds to an image of a round particle embedded in a layer of stain extending up to this midplane. In fact, particles stained on one side tend to flatten on the grid, and the stain contrast is generally relatively uniform across the image (Finch and Klug, 1965). Therefore, to simulate more uniform staining in the projection of the hemispherical models, the contrast was enhanced

toward the periphery of the model image. Contrast-adjusted projections were calculated for different symmetrical orientations of the 24-OCTA and 12-ICOSA models to compare with the symmetry averaged electron micrographs. The diameters of the symmetric 24-OCTA and 12-ICOSA models that fit the image data are 320 and 260 Å, respectively. Particles in these two categories were designated as having these dimensions, even though flattening and irregularity of staining produced images of more variable size.

Schematic computer graphics diagrams (Fig. 6, *right*), based on the models of the capsid and polymorphic shell structures (Fig. 6 *left*), were constructed to illustrate the bonding relations among the VP_1 molecules in the assembled pentamers. The packing of the pentamers was represented by arrangements of a two-dimensional pentangular figure constructed from circles on the surface of a sphere. Small adjustments in the positions of the tips of the pentangular figure were made in the diagram of the 24-capsomere shell to optimize the quasiequivalent bonding in trimers not related by a strict threefold axis.

The pictures were produced using a VAX 11/780 computer (Digital Equipment Corp., Maynard, MA), a 512-raster graphics terminal (Advanced Electronic Design, Inc., Sunnyvale, CA), and a graphics recorder (Matrix Promotions, Morris Plains, NJ).

RESULTS

Equilibria in assembly

Salient aspects of how pH, calcium, and salt concentration affect the assembly of the recombinant polyomavirus capsid protein VP_1 are illustrated by the electron micrographs in Fig. 1. The nine environmental conditions examined were attained starting with the purified VP_1 protein (molecular weight, 42,460 Da [Soeda et al., 1980]) at a concentration of 0.5–1 mg/ml in 150 mM NaCl, 15 mM 2-mercaptoethanol, 1 mM EDTA and 5% glycerol at pH 7.2, which was dialyzed in three aliquots against the solvent buffered at pH 8.5, 7.2, or 5.0. These solutions were then dialyzed against the three buffers containing 2 M $(NH_4)_2SO_4$ or 0.5 mM $CaCl_2$ without the reducing and chelating agents. Dialysis for 2 d at room temperature was adequate to reach the equilibria indicated by the arrows in Fig. 1.

In the low–ionic strength buffers containing chelating and reducing agents, the capsomeres remained unassembled at neutral and alkaline pH (Fig. 1, *d* and *e*). Above pH 10.5, the proportion of intact pentameric capsomeres decreased, presumably due to some denaturation of the protein, but in less alkaline solutions the unassembled capsomeres were stable. Upon increasing the hydrogen ion concentration to 10 μM (pH 5.0) in the low–ionic strength solution, capsomeres were assembled into capsidlike aggregates that ranged in size from ~400 Å to more than twice the normal 500 Å capsid diameter (Fig. 1 *f*). At pH 6, proton-driven formation of the variable size shells was also observed.

Addition of 0.5 mM $CaCl_2$ and removal of the EDTA and 2-mercaptoethanol at pH 8.5 led to association of some capsomeres into small (320 Å diameter) regular-shaped particles which occurred together with irregular aggregates (Fig. 1 *a*). At neutral pH, upon the addition of calcium, most of the capsomeres assembled into a relatively homogeneous population of capsidlike aggregates ranging in diameter from ~400–600 Å (Fig. 1 *b*). In the acid solution (pH 5.0), adding calcium (Fig. 1 *c*) reduced the population of free capsomeres without altering the broad size distribution of the aggregates that had previously formed on acidification (Fig. 1 *f*).

Addition of 2 M $(NH_4)_2SO_4$, with or without removal of the chelating and reducing agents, led to very similar final states of assembly at the three different hydrogen ion concentrations tested (Fig. 1, *g–i*). Capsid-like shells of diameter 400–600 Å occurred together with $T = 1$ appearing icosahedral particles of ~260 Å diameter and filiform aggregates of ~180 Å diameter. Similar small icosahedral particles were observed in CsCl density gradient fractions from cells infected with polyomavirus (Mattern et al., 1967) and SV40 (Koch et al., 1967) that may have originated by reassembly of capsomeres from disrupted normal size particles (Anderer et al., 1967). The narrow filiform aggregates, however, have not been recognized in extracts from virus-infected cells.

At high ionic strength (Fig. 1, *g–i*), the shells showed much less tendency to flatten or break apart on the grid than those formed by calcium or proton addition at low ionic strength (Fig. 1, *a–c, f*). When the high salt concentration of a specimen, such as that in Fig. 1 *h*, was lowered while adding calcium, the proportion of $T = 1$ particles and filiform aggregates was greatly reduced. Furthermore, the size distribution of the capsidlike aggregates was unchanged and these shells appeared to flatten like those assembled directly at low ionic strength (e.g., Fig. 1 *b*).

No partially formed capsids or other recognizable intermediates were observed in the early stages of the assembly processes represented in Fig. 1. The distribution of aggregates seen in preparations that were negatively stained 6 h after starting the dialyses appeared indistinguishable from the larger population of particles at equilibrium after 2 d. Disassembly of the capsidlike aggregates illustrated in Fig. 1, after dialysis back to the initial dissociating condition, was slower than the assembly process.

Other conditions for assembly that have been explored included removal of the reducing agent and prolonged incubation at intermediate salt concentrations. Limited aggregation of unassembled capsomeres, such as those in Fig. 1 *e*, occurred after dialysis to remove the 2-mercaptoethanol. Increasing the NaCl concentration to 1 M, which increases the solubility of the VP_1 (Leavitt et al., 1985), led to very gradual assembly; after 2 mo, micrographs showed a distribution of shells of diameter ranging from ~350–600 Å, together with free capsomeres. The

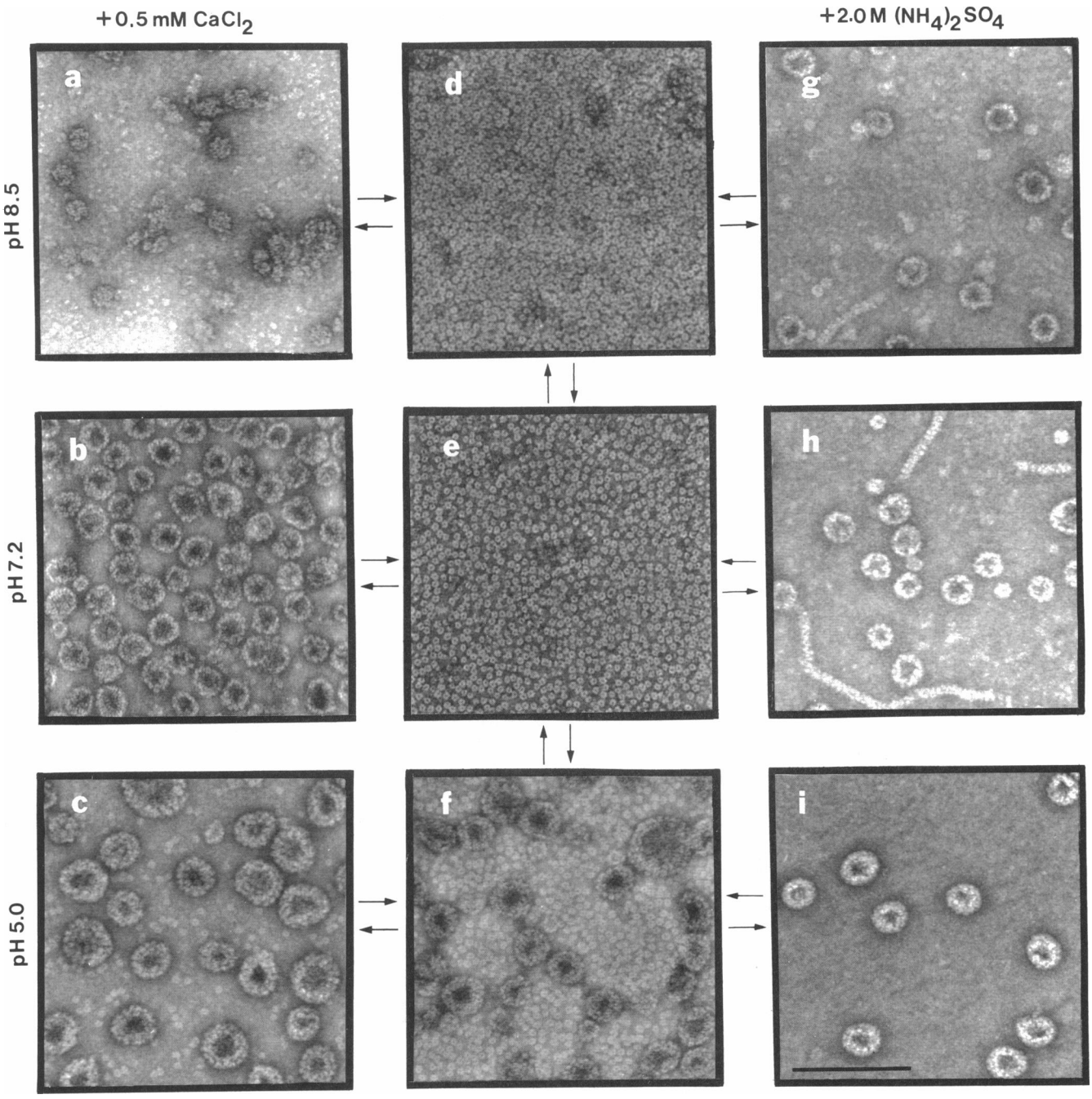

FIGURE 1 Electron micrographs of VP_1 capsomeres equilibrated under nine different solvent conditions. The micrographs are arranged in three rows according to the pH of the preparations (alkaline [*top*], neutral [*middle*], and acidic [*bottom*]), and in three columns corresponding to the initial low ionic strength solutions (*middle*) and those with added calcium (*left*) and added salt (*right*). Specimens were negatively stained with uranyl acetate after adsorption to the carbon-formvar grids for 4–5 min. The starting preparation of capsomeres was in 150 mM NaCl, 1 mM EDTA, 15 mM 2-ME, 5% glycerol buffered with 10 mM Tris-HCl at pH 7.2 (*e*), which was then dialyzed against the same solvent buffered with 10 mM Tris-HCl at pH 8.5 (*d*) or 10 mM sodium acetate at pH 5.0 (*f*). Left column (*a–c*) shows the micrographs of the VP_1 samples (*d–f*) dialyzed against the corresponding buffers containing 0.5 mM $CaCl_2$ without EDTA and 2-ME at pH 8.5 (*a*), pH 7.2 (*b*), and pH 5.0 (*c*). Right column (*g–i*) shows the micrographs of the VP_1 samples (*d–f*) dialyzed to add 2M $(NH_4)_2SO_4$ at pH 8.5 (*g*), pH 7.2 (*h*), and pH 5.0 (*i*). The grid for preparing specimen (*i*) was UV irradiated to enhance adsorption of the particles because they adhered weakly from the acid solution. Scale bar, 2,000 Å.

proportion of free capsomeres seen in these micrographs appeared to have been enhanced due to their high-affinity attachment to the carbon-coated grids, because free capsomeres were not detected by ultracentrifugation of a self-assembled VP_1 protein solution under identical solvent conditions (Salunke et al., 1986). Thus, the proportion of free capsomeres seen in Fig. 1, *c* and *f*, may have been similarly enhanced.

Pathway-dependent assembly

The structures of the aggregates formed on transition to an environment favoring assembly depend on the pathway as well as on the final conditions. Fig. 2 illustrates distinctive aggregates that formed, starting with unassembled capsomeres at pH 8.5 (Fig. 1 *d*), by adding calcium while increasing the hydrogen ion concentration. Dialyzing the alkaline solution of capsomeres against buffer at pH 7.2 containing 0.5 mM $CaCl_2$ and no chelating or reducing agent led to the formation of the relatively homogeneous population of 320-Å-diameter particles shown in Fig. 2 *a*. The inset at the bottom of Fig. 2 *a* is from a micrograph of an unstained frozen-hydrated specimen showing several 320-Å-particles, some smaller clusters of capsomeres, and one 500-Å-diameter capsidlike particle, corresponding to the aggregates seen in the negatively stained specimens. Similar populations consisting predominantly of 320-Å-diameter particles were formed from alkaline solutions adjusted up to pH 10.5 before assembly with calcium at pH 7.2. These 320-Å-diameter particles correspond to those which appear with lower frequency in the alkaline solution on calcium addition (Fig. 1 *a*). Although the final conditions of the specimens illustrated in Figs. 1 *b* and 2 *a* were the same, the 320-Å-diameter particles were not observed when calcium was added to capsomere solutions maintained at pH 7.2 as in Fig. 1 *b*. Capsomeres displayed a gradually fading memory of exposure to pH 8.5 because several days after dialysis to pH 7.2, some 320-Å particles still formed on addition of calcium to the previously alkaline preparations.

When the alkaline solution of capsomeres was dialyzed against buffer at pH 5.0 containing 0.5 mM $CaCl_2$, three distinctive types of ordered aggregates were formed (Fig.

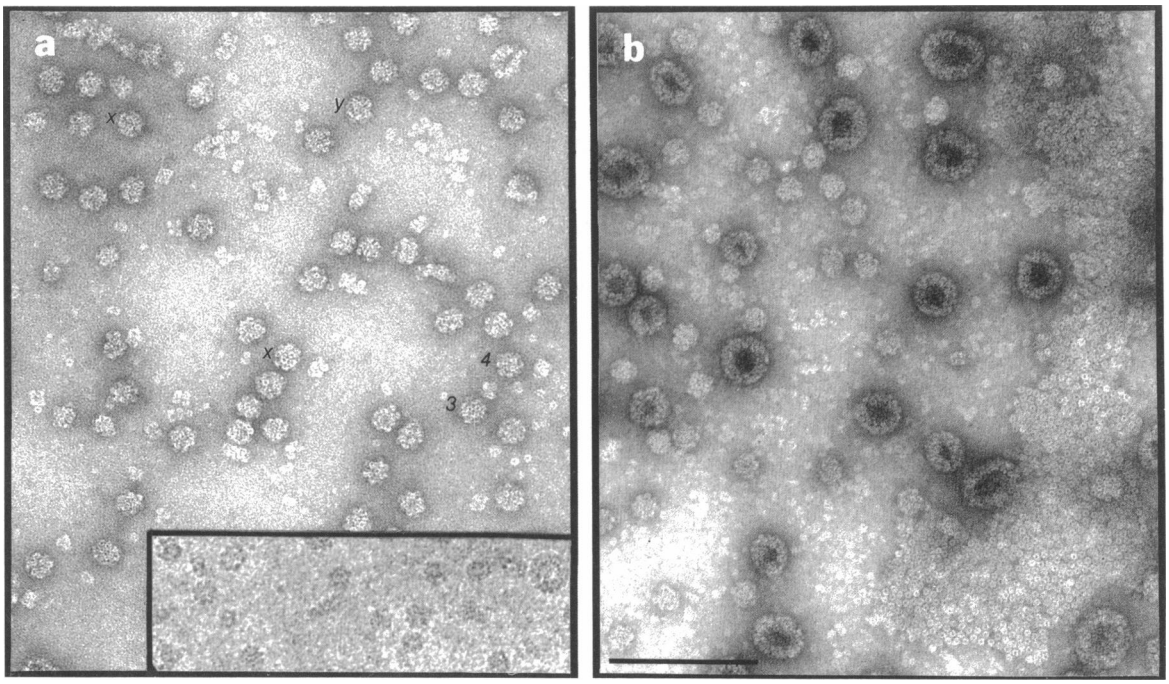

FIGURE 2 Micrographs of assemblies formed following alternate pathways to change solvent conditions. Samples in *a* and *b* were prepared starting from solutions of capsomeres at pH 8.5 (as in Fig. 1 *d*) that were dialyzed to add 0.5 mM $CaCl_2$ without EDTA and 2-ME at pH 7.2 (*a*) and pH 5.0 (*b*). The final conditions in *a* were identical to those in Fig. 1 *b* and those in *b* correspond to Fig. 1 *c*. Inset in *a* is a micrograph of an unstained frozen-hydrated sample showing a capsidlike particle with a diameter of ~500 Å (*right*) as well as smaller aggregates like those seen in the negatively stained specimen. This micrograph is representative of that used for mass measurements. The predominant uniform-sized particles in *a*, also observed in *b*, have diameters of ~320 Å. Particles of this size were not observed in the preparations assembled by calcium addition (Fig. 1 *a* and *b*) starting from pH 7.2 or 5.0 (Fig. 1, *e* and *f*, respectively). Particles of 320-Å-diameter in *a* showing three-and fourfold rotational symmetry are marked 3 and 4; two particles viewed midway between a pair of capsomeres ~24° from a fourfold axis are marked *x*; and a particle viewed near the center of a triangular facet ~13° from a twofold axis is marked *y*. Scale bar, 2,000 Å.

2 *b*: 320-Å-diameter particles, larger capsidlike shells of variable size, and extended sheets of close-packed capsomeres. The large sheet aggregates of capsomeres have not been observed under the other assembly conditions that have been examined. The variable size shells in Fig. 2 *b* correspond to those that were formed at pH 5.0, starting from pH 7.2 (Fig. 1 *f*) and that persisted with added calcium (Fig. 1 *c*). All these shells of diameter > ~400 Å show accumulation of stain in their interior. The 320-Å-diameter particles assembled from capsomeres initially at pH 8.5 by addition of calcium appear the same at pH 5.0 (Fig. 2 *b*), pH 7.2 (Fig. 2 *a*), and pH 8.5 (Fig. 1 *a*). Unlike the larger shells, the 320-Å-diameter particles show no central strain accumulation.

Comparing VP_1 preparations assembled by adding calcium at pH 7.2 starting from pH 7.2 (Fig. 1 *b*) with those starting from pH 8.5 (Fig. 2 *a*), differences were evident in the solubility as well as the appearance of the particles. The capsomere preparation at a concentration of 2 mg/ml in the 150 mM NaCl, pH 7.2 buffer (Fig. 1 *e*) was turbid due to limited solubility. When the pH was raised to 8.5 (Fig. 1 *d*), the solution cleared, indicating complete solubilization of the capsomeres under these conditions. Adding calcium to the pH 7.2 solution (Fig. 1 *b*) did not significantly increase the turbidity upon assembly of the capsidlike particles. Similarly, no loss of solubility was observed when calcium was added to the pH 8.5 solution to form the mixture of 320-Å-diameter particles and irregular aggregates (Fig. 1 *a*). In contrast, assembly starting from the soluble capsomeres at pH 8.5 by adding calcium and lowering the pH to 7.2 led to precipitation of the aggregates composed predominantly of the 320-Å-diameter particles (Fig. 2 *a*).

The 24-capsomere octahedral particle

Polymorphic shell aggregates of papovavirus capsomeres with a diameter ~60% that of the virus capsid have been observed as a minor component in preparations of rabbit papillomavirus (Finch and Klug, 1965), polyomavirus (Mattern et al., 1967), and SV40 (Koch et al., 1967). These virus-associated small particles may correspond to the distinctive 320-Å-diameter aggregate of polyomavirus VP_1 capsomeres that we have obtained. Formation of a relatively homogeneous population of the 320-Å-diameter particles (Fig. 2 *a*) indicates a unique stability under the conditions selected. Furthermore, the apparent regularity of these structures implied some well-defined symmetry and composition. Icosahedral symmetry is not possible for assemblies of >12 and <60 pentamers. Evidence of three- and fourfold symmetry in some views of the 320-Å-diameter particles (Fig. 2 *a*) suggested octahedral symmetry. Octahedral symmetry requires construction from 24 or a multiple of 24 pentamers. To determine the number of pentamers in the 320-Å-diameter particles, estimates of their mass were made from electron micrographs of unstained particles embedded in vitreous ice (Fig. 2 *a*, *bottom*).

Mass estimates from the cryoelectron micrographs were based on measurement of the integrated optical densities of different images corrected for scattering from the support medium. The corrected image density should be proportional to the net electron scattering from the ice-embedded particles; and the ratio of the numbers of electrons scattered from any pair of unstained particles with the same chemical composition should equal the ratio of their masses (Zeitler and Bahr, 1957). The average, background-corrected, integrated image density of 10 selected 320-Å-diameter particles, measured from a larger area of the micrograph of the frozen-hydrated specimen shown at the bottom of Fig. 2 *a* was about one-third (0.31 ± 0.04) that of three selected 500-Å-diameter particles. Because the 500-Å-diameter particles should consist of 72 capsomeres, this mass measurement implied that the 320-Å particles were composed of 22 ± 3 capsomeres. Thus, a 24-capsomere, octahedral structure was presumed for the 320-Å-diameter particles.

Images of presumed octahedral particles that were oriented on the grid with a symmetry axis along the direction of view were chosen for structural analysis. Four images each of views along axes of four- and threefold symmetry were selected for digital image processing, and one twofold view was identified by comparison with a model based on the four- and threefold views. Three particles viewed, respectively, along an axis of four-, three-, and twofold symmetry are shown in the top row of Fig. 3. Views along a four- or threefold axis were easy to recognize in micrographs of the specimen shown in Fig. 2 *a*, and the four selected negatively stained particles in each category appeared very similar to each other. These particles were predominantly stained on one surface and were somewhat flattened on the grid. (The stain was most likely concentrated on the surface in contact with the grid, as has been demonstrated for one-sided images of other papovaviruses [Finch and Klug, 1965].) Evaluation of the rotational power spectra (Crowther and Amos, 1971) confirmed the visually identified cyclic symmetry. Each selected image was averaged with its rotational symmetry (second row of Fig. 3) to enhance the regular features and reduce the noise. The packing arrangements of the capsomeres are evident in these four-, three-, and twofold average images. Furthermore, the symmetry-averaged images of different particles, identified as views along four- and threefold axes, showed the same features as those in Fig. 3. It was not therefore necessary to average multiple images to analyze the structure. Low-

resolution models of negatively stained particles were constructed, as described in Methods, to obtain the best fit with the symmetrically averaged images.

All the significant structural features of the symmetrically averaged micrographs in the second row of Fig. 3 correlate well with the octahedral model images in the third row. The noticeable differences in details between the micrographs and model can be explained by particle flattening and the approximations of the capsomere structure and stain distribution used in construction of the model projections. In the micrographs, the capsomeres near the center of the particles resemble the axially oriented capsomeres from dissociated preparations (e.g., Fig. 1, *d* and *e*), rather than the obliquely oriented capsomeres of the model projections. This difference can be attributed to flattening of the particles, which would result in a perpendicular orientation for the capsomeres in contact with the grid. The selected images in Fig. 3 are clearly predominantly negatively stained on one surface. Superposition of features from both the near and far sides would have obscured the structure of the individual capsomeres. Our choice of one-sided images with distinguishable capsomeres facilitated the determination of the packing arrangement. If the stain is, in fact, concentrated on the side of the particles in contact with the grid, as for other papovavirus one-sided images (Finch and Klug, 1965), then the arrangement of the 24 capsomeres in the octahedral particles that we have analyzed corresponds to the left-handed snub cube diagrammed at the bottom of Fig. 3.

Although the model shown in Fig. 3 was based on analysis of selected symmetric particle views, it accounts well for single-sided images of particles in other nonsymmetric orientations. In Fig. 2 *a*, for example, the two particles marked *x* are viewed centrally between a pair of capsomeres at the vertices of a square facet and the orientation of the particle marked *y* corresponds to a view normal to a triangular facet adjacent to a square facet of the snub cube. Thus, the flattened, single-sided images of the negatively stained particles in different orientations clearly show the snub cube packing arrangement of the capsomeres. If better quality micrographs of frozen hydrated specimens could be obtained, three-dimensional image reconstruction would provide a more comprehensive representation of the structure.

The model illustrating the surface morphology of the 24-capsomere octahedral particle in the fourth row of Fig. 3 was constructed using information about the structure and packing properties of the pentameric capsomeres from the x-ray crystallographic electron density map of the virus capsid (Rayment et al., 1982), which shows more detail than the electron micrographs in Fig. 3. This model structure, which is consistent with all the available data, corresponds to the closest packing arrangement of 24 pentagonal shaped pentamers on the surface of a sphere.

The 12-capsomere icosahedral particle

Images of the 260-Å-diameter particles that appear to be $T = 1$ icosahedral assemblies built of 12 pentameric capsomeres were analyzed using the method developed to determine the structure of the octahedral particles. This analysis was designed both to test the method and to confirm the presumed $T = 1$ structure of the small particles. Images of symmetrically oriented small particles were selected from a micrograph of VP_1 capsomeres assembled in 2 M $(NH_4)_2SO_4$ at pH 7.2, which was similar to Fig. 1 *h*. Views with two- or threefold symmetry were common and easy to recognize, but views along a fivefold axis were rare. Three of the small particles viewed, respectively, along an axis of five-, three-, and twofold symmetry are shown in the top row of Fig. 4, and, in the row below, these images have been rotationally averaged with the identified symmetry.

Construction of the icosahedral, 12-capsomere model was straightforward, because the position of the fivefold axes is fixed. The micrographs indicated that neighboring pentamers make edge-to-edge contacts corresponding to those around the pentavalent pentamer in the virion structure, but with their axes at the 63.4° angle of the icosahedron rather than the ~25° angle of the 72-capsomere icosahedral arrangement. Projections of the symmetrical views of one half of a low-resolution version of the model (Fig. 4, third row), shown in a more detailed surface view in the fourth row, are in excellent accord with the symmetrically averaged micrographs (Fig. 4, second row). Differences in appearance of corresponding details in the micrographs and model images can be accounted for by the approximations used to represent the shape of the capsomere and the stain distribution in the model projections. Comparison with the drawings of the symmetrical projections of the icosahedron at the bottom of Fig. 4 demonstrates that the 12-capsomere icosahedral particles imaged at the top of Fig. 4 are significantly stained on only one side. If the far side as well as the near side had been equally contrasted, the fivefold view would have shown a ring of ten rather than five capsomeres about the center, and the threefold view would have shown six interdigitating capsomeres rather than three in the center. The close correlation of the micrographs of these single-sided, negatively stained particles with the model images of the expected icosahedral structure shown in Fig. 4 confirms the reliability of the image analysis used to identify the octahedral particle structure shown in Fig. 3.

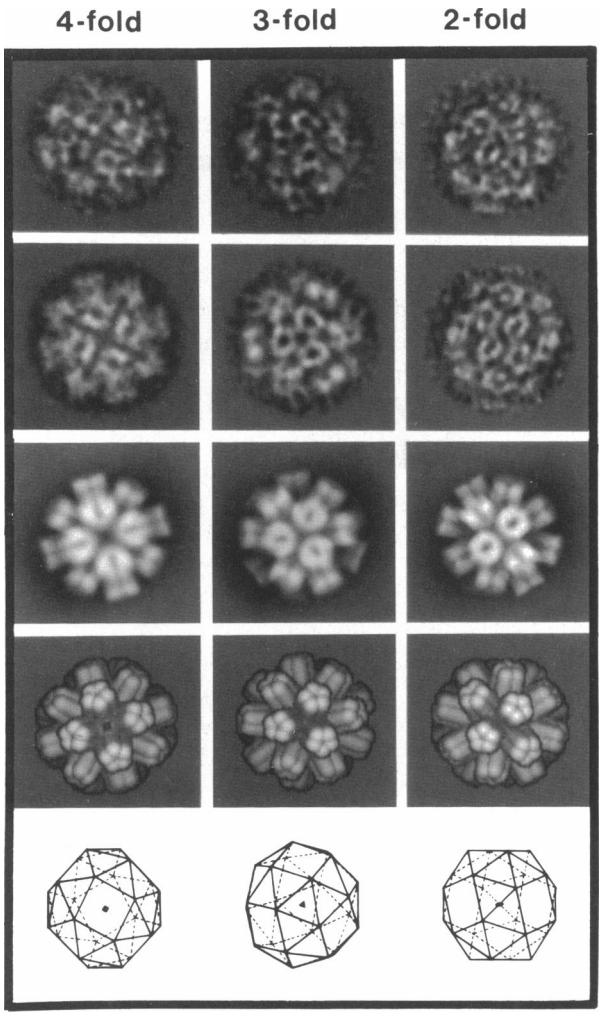

FIGURE 3 Image analysis of the 24-capsomere octahedral (24-OCTA) particle. The three columns show micrographs and models viewed along axes of four-, three-, and twofold symmetry. (*First row*) Images of three particles with the identified symmetries (selected from the larger area of the micrograph of the negatively stained specimen in Fig. 2 *a*). The fourfold view is the particle labeled 4 in Fig. 2 *a*. (*Second row*) Particle images averaged with the identified rotational symmetries. (*Third row*) Simulations of the micrographs from the projection of a low-resolution model of the 24-capsomere octahedral structure. (*Fourth row*) Illustrations of the surface morphology of the octahedral structure based on the micrographs and x-ray diffraction data for the normal capsid structure. The scaled diameter of the 24-OCTA particle is 320 Å. (*Fifth row*) Projections of the left-handed snub cube. A common twofold axis, perpendicular to the directions of view, is horizontal in all the images.

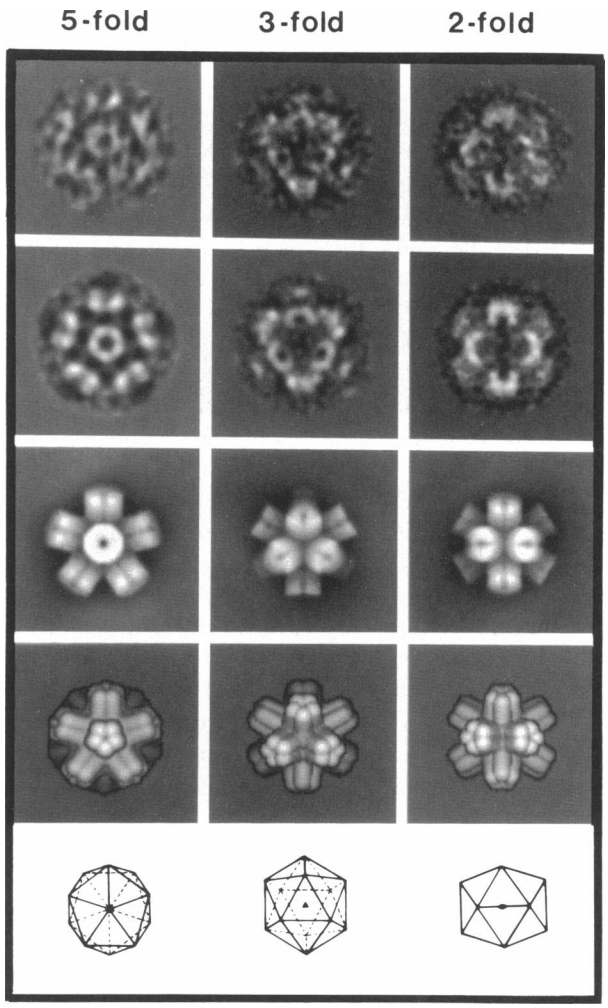

FIGURE 4 Image analysis of the 12-capsomere icosahedral (12-ICOSA) particle. The three columns show micrographs and models viewed along the axes of five-, three-, and twofold symmetry. (*First row*) Images of three particles with the identified symmetries (selected from a micrograph similar to Fig. 1 *h*). (*Second row*) Particle images averaged with the identified rotational symmetries. (*Third row*) Simulation of the micrographs from the projection of a low-resolution model of the 12-capsomere icosahedral structure. (*Fourth row*) Illustrations of the surface morphology of the icosahedral structure. The scaled diameter of the 12-ICOSA particle is 260 Å. (*Fifth row*) Projections of the icosahedron. A common twofold axis, perpendicular to the directions of view, is horizontal in all the images.

Comparison of octahedral and icosahedral assemblies

Figs. 5 and 6 summarize our analyses of the structures of the symmetric polymorphic assemblies built of 12 and 24 VP_1 capsomeres in comparison to the known structure (Rayment et al., 1982) of the icosahedral 72-capsomere polyomavirus capsid. According to the nomenclature for icosahedral surface lattices (Caspar and Klug, 1962), the icosahedral 12- and 72-capsomere shells could be designated respectively as $T = 1$ and $T = 7$. However, bonding specificity is not conserved in the 72-pentamer polyomavirus capsid, in contradiction to the quasisymmetry represented by the $T = 7$ icosahedral surface lattice design. Furthermore, the quasiequivalence theory of icosahedral virus construction provides no way to name octahedrally

symmetric shells. To identify the symmetric shells built of N_p pentameric capsomeres, without presuming bonding rules, we designate the assemblies as N_p-ICOSA and N_p-OCTA, respectively, for the icosahedral and octahedral structures. The numbers of regular pentamers mathematically allowed in shells with icosahedral symmetry are $N_p = 12$, $60n$, or $60n + 12$, where n may be any integer, and possible octahedrally symmetric shells can be built from $N_p = 24n$ pentamers. These categories do not represent a comprehensive enumeration of the surface lattices that could be built from capsomeres, although the nomenclature could be generalized to identify other symmetric assemblies. According to this system of identification, the three assemblies of pentameric capsomeres illustrated in Figs. 5 and 6 are designated 12-ICOSA, 24-OCTA, and 72-ICOSA. (To distinguish the all-pentamer shell designs from other symmetric surface lattices, the letter p could be appended to the number to specify that it denotes the number of pentamers.)

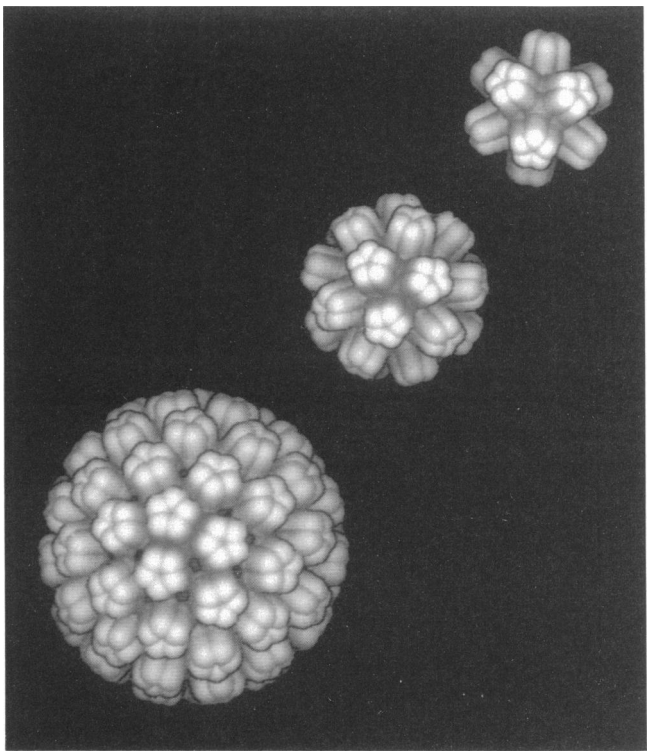

FIGURE 5 Size and morphology of the 12-ICOSA, 24-OCTA, and 72-ICOSA assemblies. The diameter of the 72-capsomere icosahedral (72-ICOSA) virus capsid is 500 Å, and the scaled diameters of the 24-capsomere octahedral (24-OCTA) and 12-capsomere icosahedral (12-ICOSA) particles are 320 and 260 Å, respectively. The 72-ICOSA model is viewed near a quasi-threefold axis and the 24-OCTA and 12-ICOSA models are viewed along strict threefold axes. Similar trimer contacts are made among the three capsomeres at the center of each picture, but the angles between neighboring pentamer axes are 63.4, 43.7, and ~25°, respectively, for the 12-ICOSA, 24-OCTA, and 72-ICOSA particles.

The stylized model of the 72-ICOSA structure illustrated in Figs. 5 and 6 was constructed (Salunke et al., 1986) to conform closely to the 22-Å resolution electron density map of the polyomavirus capsid (Rayment et al., 1982). The capsomeres in the 12-ICOSA and 24-OCTA models were assumed to have the same structure as in the 72-ICOSA capsid model. Analysis of the images from the electron micrographs (Figs. 3 and 4) established the symmetry of the capsomere packing and the overall dimensions. The pentamer orientations in the 12-ICOSA and 24-OCTA models were adjusted, within the limits allowed by the image analysis, to avoid interpenetration and to obtain packing relations among the capsomeres that were most consistent with those identified in the virus capsid. The orientations illustrated in the 12-ICOSA and 24-OCTA models represent the closest possible packings for 12 and 24 pentagons, respectively, arranged on spherical shells. Any other spherical arrangements of 12 and 24 noninterpenetrating, identical capsomeres with the dimensions illustrated in Fig. 5 would lead to larger particle diameters than those determined from the micrographs.

Fig. 5 illustrates the relative sizes of the 12-ICOSA, 24-OCTA, and 72-ICOSA shells with outer diameters of 260, 320, and 500 Å, respectively. In each shell, the capsomeres make contact with their neighbors in a spherical surface of diameter ~110–120 Å less than the outer particle diameter. Thus, the protruding domain of each capsomere extends radially outward ~55–60 Å from the surface of close contact. Because the overall length of the capsomere in the radial direction is ~80 Å, the thickness of the portion forming the closely packed shells is ~20–25 Å. Although the same portion of the capsomere is involved in the bonding that holds the different shells together, the angles between neighboring pentamer axes differ substantially according to shell size: this angle is 63.4° for 12-ICOSA, 43.7° for 24-OCTA, and ~25° for 72-ICOSA.

The similarities and differences of the capsomere arrangements in the 12-ICOSA, 24-OCTA, and 72-ICOSA shells are illustrated by the stereo pictures and spherical packing diagrams in Fig. 6. The scaled diameters of the three spherical surfaces where the capsomeres make contact are ~140, 200, and 380 Å, which are roughly in the ratios $1:\sqrt{2}:\sqrt{7}$. If the capsomeres were equally close packed, the ratios of the diameters of the three shells would be in proportion to the square roots of the number of capsomeres in each shell, which is $1:\sqrt{2}:\sqrt{6}$. Thus, the packing is less tight in the 72-ICOSA shell than in the 12-ICOSA and 24-OCTA shells. The structural basis for this difference in compaction is evident from comparison of the schematic packing diagrams

in Fig. 6. In the 12-ICOSA assembly, each pentagonal unit makes equivalent edge-to-edge contacts with five neighbors, corresponding to the arrangement of the faces of the pentagonal dodecahedron, in which three corners are equivalently joined at each icosahedral threefold axis. There is no way in which more than 12 regular pentagons can be tightly packed in any surface to make trimer connections at each corner. In the 24-OCTA assembly, the tips of four of the five molecules in the pentamer make trimer connections, involving some small quasiequivalent adjustments in their position, but the fifth molecule, facing toward the fourfold axis, is unconnected. In the 72-ICOSA assembly, of the six VP_1 molecules in the icosahedral asymmetric unit (one hexavalent pentamer and one-fifth of a pentavalent pentamer), only three form trimer connections in the more open arrangement that is geometrically imposed for packing the larger number of pentagonal units on a spherical surface.

DISCUSSION:

Octahedral symmetry was not anticipated for polymorphic assemblies of polyomavirus capsomeres. Cubic symmetry had been predicted for the protein shells of spherical shaped viruses by Crick and Watson (1956) on the presumption that these structures should be built from a large number of identical small protein molecules packed together in a regular manner. Their postulate of regular packing had not suggested any preference among the three possible classes of cubic symmetry (namely, tetrahedral, octahedral, and icosahedral, which mathematically require 12, 24, and 60 asymmetric units, respectively). On the assumption that bonding specificity would be conserved for multiple copies of a structural protein in the asymmetric unit, the quasiequivalence theory (Caspar and Klug, 1962) predicted that isometric virus particles should have icosahedral symmetry. So far, the well-characterized isometric virus particles have all turned out to be icosahedral, even though the quasiequivalence rules are not always observed (Rayment et al., 1982). Octahedral symmetry had been inferred for satellite tobacco necrosis virus from an analysis of x-ray crystallographic data (Akervall et al.,1971), but this was shown to be a misinterpretation of the rotation function calculated for the crystals of this icosahedral virus (Klug, 1971). Since then, the possibility of octahedral symmetry in virus structures has not been seriously considered. Our discovery of an octahedral aggregate of polyomavirus capsomeres, consisting of 120 VP_1 molecules, demonstrates that octahedral virus capsids could exist. The prevalence of icosahedral virus symmetry may be more a result of evolutionary history rather than the manifestation of an underlying mathematical principle. Whether or not the structures formed by polyomavirus capsomeres exemplify unifying design concepts, comparison of their symmetry and stability can provide critical information about the mechanics of the assembly process.

Conserved connections

The basic building block in the polymorphic assemblies is the VP_1 pentamer because its internal structure appears invariant under diverse conditions of association or dissociation. Similarities in the packing arrangements of polyomavirus capsomeres in different assemblies suggest homologies in the bonding interactions; and the large differences in curvature among the various shells imply flexibility in these bonds. Switching in bonding specificity is required to build the virus capsid (Rayment et al., 1982; Salunke et al., 1986), and this switching may be related to the capacity of the pentamers to form a variety of ordered polymorphic aggregates.

Three different bonding states have been distinguished for the six VP_1 molecules in the icosahedral asymmetric unit of the 72-ICOSA virus capsid structure (Rayment et al., 1982; Salunke et al., 1986). Representing the cross-sectional boundary of the capsomere in the surface of contact by a pentangular shaped outline (Fig. 6), the three bonding states, designated by the letters **a, b,** and **c** in Fig. 6 *c*, correspond respectively to connection of three tips, two tips, and a pair of overlapped corners of the pentamers. In the 12-ICOSA and 24-OCTA structures illustrated in Fig. 6, *a* and *b*, only trimer connections of the tips occur. Junction of the pentamer tips in trimers and dimers also occur in the polymorphic tube assemblies of polyomavirus capsomeres (Baker et al., 1983). There must be flexibility in these connections, because the angles between neighboring pentamer axes range from 63.4° in the 12-ICOSA structure (Fig. 6 *a*) to ~25° in the 72-ICOSA structure (Fig. 6 *c*) and to smaller angles in larger diameter shell and sheet assemblies (Figs. 1, *c* and *f*, and 2 *b*). All pentamer tips form equivalent trimer connections in the 12-ICOSA structure (Fig. 6 *a*), but in any larger assembly, some pentamer tips will either remain unconnected, as in Fig. 6 *b*, or may be connected in pairs, as in Fig. 6 *c*. Within the range of energetically allowed packing angles, the most stable packing arrangements in the surface lattices appear to be those which maximize the tip-to-tip contacts among pentamers.

Stabilizing interactions in assembly

Our observations on the conditions which favor assembly of the recombinant VP_1 pentamers complement the investigations of the conditions for dissociation of intact virions (Brady et al., 1977; Friedman and David, 1972). The

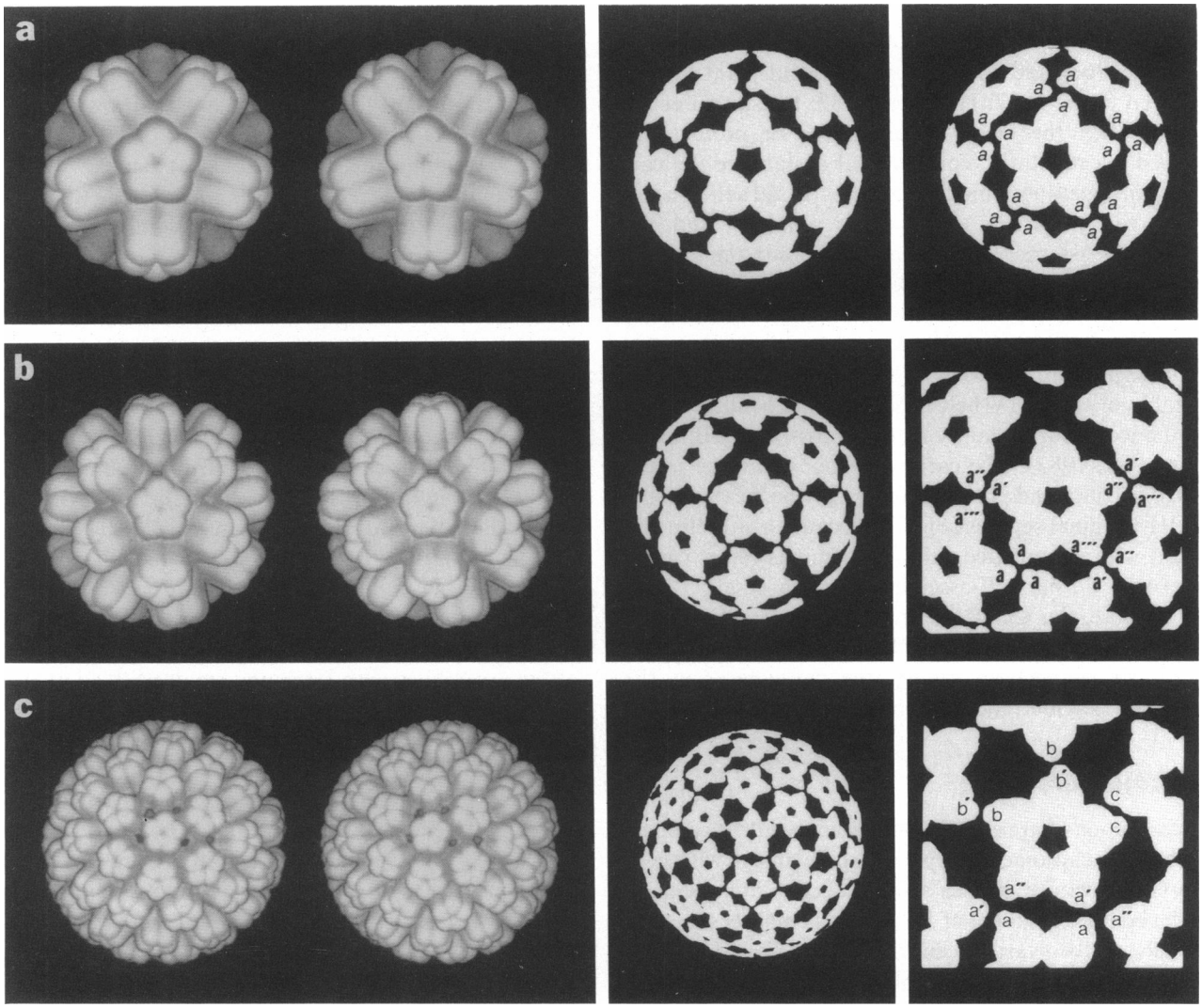

FIGURE 6 Comparison of VP_1 bonding relations in the 12-ICOSA (*a*), 24-OCTA (*b*), and 72-ICOSA (*c*) capsomere assemblies. The stereo-pair pictures (*left*) are shown with decreasing magnification to produce equal size images for the 260-, 320-, and 500-Å-diameter particles (top, middle, and bottow rows, respectively). The schematic diagrams (column right of center) illustrate the packing arrangements of the pentameric capsomeres in spherical surfaces of close packing for the 12-ICOSA, 24-OCTA, and 72-ICOSA shells. The outside ends of the projecting capsomere domains in each of the assemblies are ~60 Å above the contact surfaces (as indicated in the stereo-pictures): thus, the scaled diameters of the three shells at the levels of close packing are ~140, 200, and 380 Å. In the far right column, the bonding states of the VP_1 molecules in the central pentamers of each schematic shell diagram (all displayed at the same scale) are indicated by the letters marking the interacting tips of the pentangular capsomere cross-sections. The letter **a** designates VP_1 bonding regions that form trimer connections: Three different type faces are used to differentiate the trimer bonding in 12-ICOSA, 24-OCTA, and 72-ICOSA, and the primes distinguish quasiequivalently related VP_1 bonding tips in 24-OCTA and 72-ICOSA. In the diagram for 72-ICOSA, the letters **b** and **c** designate dimer bonding sites connecting subunit tips related by a quasidiad (**b–b'**) and overlapped corners related by a strict diad (**c–c**).

dependence of the stability on pH, calcium concentration, and ionic strength demonstrates the importance of electrostatic interactions in the assembly and disassembly processes. Disulfide links may also contribute to the stability of the assembled capsid (Walter and Deppert, 1974). Removal of the reducing agent from a preparation of unassembled capsomeres, such as that in Fig. 1 *e*, led to some limited association, indicating that oxidation may stabilize capsidlike assemblies. However, because capsomeres can form capsidlike structures at high ionic strength in the presence of the reducing agent, disulfide links do not appear to be necessary for assembly.

Assembly of capsomeres on addition of calcium (Fig. 1 *a* and *b*) or protons (Fig. 1 *f* can be accounted for by the binding of these positively charged ions to closely apposed carboxyl pairs in the assembled struc-

tures. Carboxyl pairs provide a sensitive electrostatic switch that controls the assembly of tobacco mosaic virus (Caspar, 1963) and the small icosahedral plant viruses (Durham et al., 1977; Harrison, 1980; Rossmann et al., 1983). When the bound calcium ions or protons are removed, electrostatic repulsion will destabilize the carboxyl pairing at low ionic strength. Increased salt concentration will shield the electrostatic repulsion and can stabilize the assembly in alkaline solutions in the absence of calcium. The carboxyl pairs, presumed to form during assembly under physiological conditions, could directly link VP_1 molecules in adjacent capsomeres, analogous to the intermolecular carboxyl pairing that stabilizes assembly of the TMV helix (Namba and Stubbs, 1986) and the icosahedral plant viruses (Harrison, 1980; Rossmann et al., 1983). The carboxyl groups involved in the critical calcium and proton binding may be located in the COOH-terminal segment of VP_1, because a site-directed mutant with a truncated carboxy terminus forms capsomeres that do not self-assemble (Garcea et al., 1987). Furthermore, this COOH-terminal segment of VP_1 could form part of the structure involved in making the trimer and dimer connections among the capsomeres in the capsid and polymorphic assemblies.

Variable curvature

The formation of apparently similar noncovalent contacts between the capsomeres in polymorphic arrays with very different curvature implies some hingelike link connecting the bonding segment of VP_1 at the pentamer tips with the structurally invariant central domain. Variation in the packing angle between neighboring capsomeres under different conditions may result from some locally induced conformational change in the "hinge," or, alternatively, the hinge bending could be an indirect consequence of long-range electrostatic forces that are altered by changes in pH or ionic strength.

Electrophoretic measurements on virions and capsids (Thorne et al., 1965) have shown that the outwardly projecting surface of the capsomere is negatively charged in neutral and alkaline solutions. Titration of the negatively charged carboxyl groups on the outer surface may account for the formation of large diameter shell and sheet assemblies in acid solution (Figs. 1, *c* and *f*, and 2 *b*), because the reduced electrostatic repulsion between neighboring projecting domains could allow more nearly parallel alignment of neighboring capsomere axes. Conversely, the increased negative charge on the outer surface in alkaline solutions may contribute to the preferential formation of the 320-Å-diameter 24-OCTA shells (Figs. 1 *a* and 2, *a* and *b*), because the 43.7° angle between neighboring capsomere axes increases the separation of their outer ends, compared with the packing in large diameter shells. This steeper packing angle may also be favored by some pH-dependent, metastable conformational change in VP_1, because the potential of the protein to form the 24-OCTA shells displayed a transient memory of previous exposure to alkaline solutions.

The capsidlike shells, assembled at neutral pH with 1 M NaCl (Salunke et al., 1986) and higher salt concentrations (Fig. 1, *g–i*), or with calcium addition at physiological ionic strength (Fig. 1 *b*), have diameters of 400–600 Å corresponding to packing angles between capsomere axes in the range ~30–20°. Thus, the balance of forces among the VP_1 capsomeres under these in vitro conditions is not sufficiently restrictive to determine a unique assembly. Precise assembly of the VP_1 pentamers with a 25° packing angle in the 72-ICOSA virus capsid presumably requires accessory control mechanisms.

The formation of the 260-Å-diameter 12-ICOSA and 180-Å-diameter filiform aggregates in 2 M $(NH_4)_2SO_4$, together with the predominant 400–600-Å-diameter capsidlike shells (Fig. 1, *g* and *h*), might result from changes in the kinetics of assembly of the arrays with different curvature as the ionic strength is increased. Coexistence of the assemblies with large and small packing angles is not a likely equilibrium property of the capsomere bonding, because the small diameter aggregates dissociate preferentially at lower salt concentrations, even in the presence of calcium which stabilizes the capsidlike shells. These differences in stability may be related to the conformational changes in the interacting tips of the capsomeres packed together at different angles to each other.

Pentamer packing geometry

Geometrically, the design of the assemblies of pentameric capsomeres can be described in terms of packing arrangements of regular pentagons. Arrangements which maximize the trimer connections among pentagon corners are close packed. Finding compact arrangements of N pentagons that will form isometric shells is analogous to determining the closest packing of N circles or spheres on the surface of a larger sphere. This packing problem is mathematically difficult and has been solved without symmetry restrictions only for relatively small values of N (Fejes Tóth, 1952). Tarnai and Gáspár (1987) have found closest packing arrangements for large values of N, restricted to arrangements with tetrahedral, octahedral, and icosahedral symmetry. They have shown, surprisingly, that 72 circles on a spherical surface can be packed more closely with octahedral rather than icosahedral symmetry. The compact 72-OCTA structure represents a plausible polymorphic assembly of polyomavirus VP_1 pentamers which has more trimer connections than the 72-ICOSA structure. The arrangements of the capso-

meres in many of the polymorphic assemblies that we have observed may correspond to mathematically predicted symmetric close packing arrangements of circles on the surface of a sphere. Derivation of geometrical models for shells consisting of close-packed pentagons should, therefore, prove useful in further analysis of the structures of polymorphic papovavirus assemblies.

Polymorphic shell and tube aggregates of capsomeres have been observed in extracts of cells infected with all the papovaviruses that have been investigated (rabbit papilloma and human wart viruses: Finch and Klug, 1965; Kiselev and Klug, 1969; polyomavirus: Mattern et al., 1967; SV40: Koch et al., 1967). Presuming that all the virus-associated shells are built of pentameric capsomeres, those intermediate in size between the 12- and 72-capsomere icosahedral shells cannot have icosahedral symmetry. The intermediate-sized shells, with diameters of ~60 and 80% that of the normal capsid, appear to have a regular structure which could consist of 24 and 48 octahedrally arranged pentamers, respectively. A rare class of tube formed by polyomavirus capsomeres has a square surface lattice arrangement of the pentamers (Baker et al., 1983) that may be closely related to the octahedral shell designs. If, in fact, the variant octahedral structures occur naturally, they could be stabilized by a tetrameric reagent designed to bind selectively to the four unoccupied VP_1 bonding sites facing each fourfold axis. Such a reagent might interfere with virion assembly without impeding normal cell functions. Thus, further studies on conditions for stabilizing octahedral assemblies of papovavirus capsomeres could lead to applications for blocking assembly of infectious papillomaviruses.

We thank Linda Melanson for the electron microscopy of the frozen-hydrated specimens, Bernie Stallmeyer for assistance in the use of the Spider software, Michael Clarage for help with the computer graphics, Lynn Montross and Marguerite Cahoon for technical assistance, Judy Black for the photography, and Louise Seidel and Beth Finkelstein for help in preparing the manuscript.

This investigation was supported by United States Public Health Service grants CA 15468 and CA47439 to D. L. D. Caspar and CA37667 to R. L. Garcea from the National Cancer Institute, Department of Health and Human Services, and a Junior Faculty Award JFRA158 to R. L. Garcea from the American Cancer Society.

Received for publication 4 March 1989 and in final form 7 July 1989.

REFERENCES

Akervall, K., B. Strandberg, M. G. Rossmann, U. Bengtsson, K. Fridborg, H. Johannisen, K. K. Kannan, S. Lövegren, G. Petef, B. Oberg, D. Eaker, S. Hjertén, L. Rydén, and I. Moring. 1971. X-Ray diffraction studies of the structure of satellite tobacco necrosis virus. *Cold Spring Harbor Symp. Quant. Biol.* 36:469–483.

Anderer, F. A., H. D. Schlumberger, M. A. Koch, H. Frank, and H. J. Eggers. 1967. Structure of Simian virus 40. II. Symmetry and components of the virus particle. *Virology.* 32:511–523.

Argos, P., and J. E. Johnson. 1984. Chemical stability in simple spherical plant viruses. *In* Biological Macromolecules and Assemblies. Vol. 1. Virus Structures, F. A. Jurnak and A. McPherson, editors. Wiley & Sons, New York. 1–43.

Baker, T. S., D. L. D. Caspar, and W. T. Murakami, 1983. Polyoma virus "hexamer" tubes consist of paired pentamers. *Nature (Lond.).* 303:446–448.

Bancroft, J. B. 1970. The self-assembly of spherical plant viruses. *Adv. Virus Res.* 16:99–134.

Bloomer, A., and P. J. G. Butler. 1986. Tobacco mosaic virus structure and self-assembly. *In* The Plant Viruses. Vol. 2. M. H. V. Van Regenmortel and H. Fraenkel-Courat, editors. Plenum Publishing Corp., New York. 19–57.

Brady, J. N., V. D. Winston, and R. A. Consigli. 1977. Dissociation of polyomavirus by the chelation of calcium ions found associated with purified virions. *J. Virol.* 23:717–724.

Caspar, D. L. D. 1963. Assembly and stability of the tobacco mosaic virus particle. *Adv. Protein Chem.* 18:37–121.

Caspar, D. L. D., and A. Klug. 1962. Physical principles in the construction of regular viruses. *Cold Spring Harbor Symp. Quant. Biol.* 27:1–24.

Christiansen, G., T. Landers, J. Griffith, and P. Berg. 1977. Characterization of components released by alkali disruption of Simian virus 40. *J. Virol.* 21:1079–1084.

Crick, F. A. C., and J. D. Watson. 1956. Structure of small viruses. *Nature (Lond.).* 177:473–476.

Crowther, R. A., and L. A. Amos. 1971. Hamonic analysis of electron microscope images with rotational symmetry. *J. Mol. Biol.* 60:123–130.

Dubochet, J., M. Adrian, J.-J. Chang, J.-C. Homo, J. LePault, A. W. McDowall, and P. Schultz. 1988. Cryo-electron microscopy of vitrified specimens. *Q. Rev. Biophys.* 21:129–228.

Durham, A. C. H., D. A. Hendry, and M. B. Von Wechman. 1977. Does calcium ion binding control plant virus disassembly? *Virology.* 77:524–533.

Fejes Tóth, L. 1952. Lagerungen in der Ebene auf der Kugel und im Raum. Springer-Verlag, Berlin.

Finch, J. T., and A. Klug. 1965. Structure of viruses of the papilloma-polyoma type. III. Structure of rabbit papilloma virus. *J. Mol. Biol.* 13:1–12.

Frank, J., B. Shimkin, and H. Dowse. 1981. Spider: a modular software system for electron image processing. *Ultramicroscopy.* 6:343–358.

Friedman, T., and D. David. 1972. Structural role of polyoma virus proteins. *J. Virol.* 10:776–782.

Garcea, R. L., D. M. Salunke, and D. L. D. Caspar. 1987. Site directed mutations affecting polyomavirus capsid self-assembly *in vitro*. *Nature (Lond.).* 329:86–87.

Harrison, S. C. 1980. Protein interfaces and intersubunit bonding. The case of tomato bushy stunt virus. *Biophys. J.* 32:139–153.

Kiselev, N. A., and A. Klug. 1969. The structure of viruses of the papilloma-polyoma type. V. Tubular variants built of pentamers. *J. Mol. Biol.* 40:155–171.

Klug, A. 1965. Structure of viruses of the papilloma polyoma type. II. Comments on other work. *J. Mol. Biol.* 11:424–431.

Klug, A. 1971. Interpretation of the rotation function map of satellite tobacco necrosis virus: octahedral packing of icosahedral particles. *Cold Spring Harbor Symp. Quant. Biol.* 36:483–487.

Koch, M. A., H. J. Eggars, F. A. Anderer, H. D. Schlumberger, and H. Frank. 1967. Structure of Simian virus 40. I. Purification and physical characterization of the virus particle. *Virology*. 32:503–510.

Leavitt, A. D., T. M. Roberts, and R. L. Garcea. 1985. Polyomavirus major capsid protein VP_1: purification after high level expression in *Escherichia coli*. *J. Biol. Chem.* 260:12803–12809.

Mattern, C. T. F., K. K. Takemoto, and A. DeLeva. 1967. Electron microscopic observations on multiple polyomavirus related particles. *Virology*. 32:378–392.

Namba, K., and G. Stubbs. 1986. Structure of tobacco mosaic virus at 3.6 Å resolution: implications for assembly. *Science (Wash. DC)*. 231:1401–1406.

Namba, K., D. L. D. Caspar, and G. Stubbs. 1988. Enhancement and simplification of macromolecular images. *Biophys. J.* 53:469–475.

Okada, Y. 1986. Molecular assembly of tobacco mosaic virus *in vitro*. *Adv. Biophys.* 22:95–145.

Rayment, I., T. S. Baker, D. L. D. Caspar and W. T. Murakami. 1982. Polyoma virus capsid structure at 22.5 Å resolution. *Nature (Lond.)*. 295:110–115.

Rossmann, M. G., C. Abad-Zapatero, M. A. Hermodson, and J. W. Erickson. 1983. Subunit interactions in southern bean mosaic virus. *J. Mol. Biol.* 166:37–83.

Salunke, D. M., D. L. D. Caspar, and R. L. Garcea. 1986. Self-assembly of purified polyomavirus capsid protein VP_1. *Cell*. 46:895–904.

Soeda, E., J. F. Arrand, and B. E. Griffin. 1980. Polyoma virus DNA: complete nucleotide sequence of the gene which codes for polyoma virus capsid protein VP_1 and overlaps the VP_2/VP_3 genes. *J. Virol.* 33:619–630.

Tarnai, T., and Zs. Gáspár. 1987. Multi-symmetric close packings of equal spheres on the spherical surface. *Acta Crystallogr. Sect. A*. 43:612–616.

Thorne, H. V., W. House, and A. L. Kisch. 1965. Electrophoretic properties and purification of large and small plaque-forming strains of polyoma virus. *Virology*. 27:37–43.

Walter, G., and W. Deppert. 1974. Intermolecular disulfide bonds: an important structural feature of the polyoma virus capsid. *Cold Spring Harbor Symp. Quant. Biol.* 39:255–257.

Zeitler, E., and G. F. Bahr. 1957. Contributions to the quantitative interpretation of electron microscope pictures. *Exp. Cell Res.* 12:44–65.